Journal of Sound and Vibration (1998) **217**(2), 239–260
Article No. sv981748

SOUND INSERTION LOSS OF STIFFENED ENCLOSURE PLATES USING THE FINITE ELEMENT METHOD AND THE CLASSICAL APPROACH

Y.-Y. LEE

Department of Aerospace Engineering, Old Dominion University, Norfolk, VA 23529-0247 *U.S.A.*

AND

C. F. NG

Department of Civil and Structural Engineering, The Hong Kong Polytechnic University, Hung Hom, Kowloon, Hong Kong

(*Received* 14 *January* 1998, *and in final form* 28 *April* 1998)

This paper reports a theoretical and experimental study of insertion loss of stiffened enclosure plates which are used for noise control in industrial machines, automobiles, trains and aircrafts. The theoretical analysis is based on the finite element method in [1] for the structural part, and the classical solution suggested in [2, 3] for the acoustic part. The effects of boundary conditions, acoustic resonance and structural resonance on the insertion loss are studied. The theoretical results agree reasonably well with the experimental results. Both numerical and experimental results point to two important findings: 1) the coupling effect between the (1, 0) acoustical mode and the (2, 1) structural mode is an important factor which can cause deterioration of the insertion loss of an enclosure plate; and 2) stiffeners can be used to enhance the insertion loss ability of an enclosure plate at the frequencies below the fundamental resonance. However, at other frequencies, the enclosure plate could give worse insertion loss performance.

1. INTRODUCTION

This paper reports a theoretical and experimental study of insertion loss of stiffened enclosure plates which are used for noise control in industrial machines, automobiles, trains and aircrafts. Lee [2–6], Lyon [7], Pretlove [8], Jackson [9], Guy [10], Dowell [11], Narayanan [12] and Oldham [13, 14] have investigated the vibration and sound coupling characteristics of enclosure panels using the modal analysis or Fourier transform methods to model the structural–acoustic coupling enclosure models. So far, they have mainly considered modal analysis techniques for solving the problem of sound and vibration with analytical relationships between various parameters.

0022–460X/98/420239 + 22 $30.00/0

The models of Lyon [7], Pretlove [8], Guy [10], Dowell [11] and Narayanan [12] consisted of only one flexible plate which was used to simulate an enclosure panel and driven by external sound pressure, and five rigid walls. Thus, their models were presented only for predicting the sound pressure transmission from the outside to the inside of the enclosure model. Usually, the most significant measure for acoustic performance of an enclosure is the sound insertion loss, produced by the difference between the measured sound pressure level outside the enclosure at a specific point with and without the enclosure fitted to a noise source. The sound insertion loss is more preferable than other parameters for enclosure design and analysis as most enclosures are designed to reduce noise level at some particular location or specified region. At the same time, evaluation of insertion loss pertains only to measurements in sound pressure levels external to the enclosure that can be obtained without difficulties. Therefore, this is an important reason why the models should be further improved so as to be more realistic and practical. The enclosure models of Jackson [9] and Oldham [13], which were used for predicting the insertion loss, cannot handle any estimation of the effects of the cavity resonance in a direction parallel to the source plate. Besides, as mentioned in their paper, Oldham's formula is valid only in the case of the source plate vibrating in symmetric mode shapes; and Jackson's formula cannot predict the effect of the vibration mode shape of the noise source.

In references [2–5, 7–14], the authors adopted the classical plate theory for the structural parts in their structural–acoustic analysis. Reddy [15] reviewed the application of finite element methods to plate problems. The finite element method is more powerful and versatile for structural problems of complex geometries, boundary conditions, and loadings, when compared with classical solutions. Most of the classical continuum solutions of plates have been limited to a single mode approximation. This is due to the difficulties in obtaining the general multiple mode governing equations using the Galerkin approach, especially for plates with complex boundary conditions or stiffeners. Thus, in this paper, the theoretical analysis is based on the finite element method in reference [1] for the structural part, and the classical solution suggested in reference [3] for the acoustic part. The effects of stiffeners, boundary conditions, acoustic resonance and structural resonance on the insertion loss, are studied. The comparison between numerical and experimental results shows the validity of the theoretical model.

2. ISOPARAMETRIC PLATE ELEMENT

The *in-vacuo* mode shapes of the source plate and the enclosure plate in Figure 1 are found by using the finite element. The four-node C^1 conforming rectangular plate element in reference [16] is chosen in the finite element model. The element has a total of 24 degrees of freedom (16 bending and 8 membrane). The displacements within the element can be expressed as

$$u = b_1 + b_2x + b_3y + b_4xy, \qquad v = b_5 + b_6x + b_7y + b_8xy \Rightarrow \begin{Bmatrix} u \\ v \end{Bmatrix} = \begin{bmatrix} \lfloor \mathbf{H}_u \rfloor \\ \lfloor \mathbf{H}_v \rfloor \end{bmatrix} \{\mathbf{b}\}; \tag{1a}$$

$$w = a_1 + a_2x + a_3y + a_4x^2 + a_5xy + a_6y^2 + a_7x^3 + a_8x^2y + a_9xy^2 + a_{10}y^3 + a_{11}x^3y + a_{12}xy^3 + a_{13}x^2y^2 + a_{14}x^3y^2 + a_{15}x^2y^3 + a_{16}x^3y^3$$

$$\Rightarrow w = \lfloor \mathbf{H}_w \rfloor \{\mathbf{a}\}, \tag{1b}$$

where w, u and v are the transverse and membrane displacements. Combining equations (1a) and (1b) gives

$$\begin{Bmatrix} u \\ v \\ w \end{Bmatrix} = \begin{bmatrix} \begin{bmatrix} \mathbf{H}_u(x, y) \\ \mathbf{H}_v(x, y) \end{bmatrix} [\mathbf{T}_m] & [\mathbf{0}] \\ [\mathbf{0}] & [\mathbf{H}_w(x, y)][\mathbf{T}_b] \end{bmatrix} \begin{Bmatrix} \mathbf{w}_m \\ \mathbf{w}_b \end{Bmatrix}, \tag{2}$$

where

$$\{\mathbf{b}\} = [\mathbf{T}_m]\{\mathbf{w}_m\}, \qquad \{\mathbf{a}\} = [\mathbf{T}_b]\{\mathbf{w}_b\},$$

$\{\mathbf{w}_m\}$ = membrane displacements at the four nodal points

$$= \lfloor u_1 \quad v_1 \quad u_2 \quad v_2 \quad u_3 \quad v_3 \quad u_v \quad v_4 \rfloor^{\mathrm{T}}$$

$\{\mathbf{w}_b\}$ = bending displacements at the four nodal points

$$= \lfloor w_1 \quad w_2 \quad w_3 \quad w_4 \quad w_{1,x} \quad w_{2,x} \quad w_{3,x} \quad w_{4,x} \quad w_{1,y} \quad w_{2,y} \quad w_{3,y} \quad w_{4,y} \quad w_{1,xy} \quad w_{2,xy} \quad w_{3,xy} \quad w_{4,xy} \rfloor^{\mathrm{T}}$$

The subscripts m and b represent membrane and bending respectively. Details of $[\mathbf{T}_m]$ and $[\mathbf{T}_b]$ can be found in the appendix.

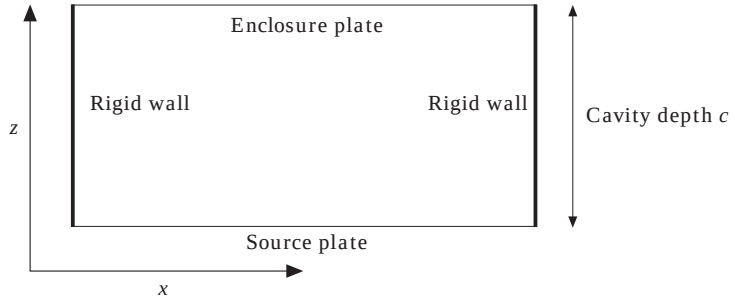

Figure 1. Side view of rectangular enclosure model.

From the above equations, the stiffness matrix for the plate element can be formulated in the form

$$[\mathbf{k}_p] = \int_{Area_p}\int \begin{bmatrix} [\mathbf{C}_m][\mathbf{T}_m] & [\mathbf{0}] \\ [\mathbf{0}] & [\mathbf{C}_b][\mathbf{T}_b] \end{bmatrix}^{\mathrm{T}} \begin{bmatrix} [\mathbf{A}_p] & 0 \\ 0 & [\mathbf{D}_p] \end{bmatrix} \begin{bmatrix} [\mathbf{C}_m][\mathbf{T}_m] & [\mathbf{0}] \\ [\mathbf{0}] & [\mathbf{C}_b][\mathbf{T}_b] \end{bmatrix} \mathrm{d}x\ \mathrm{d}y, \tag{3}$$

where

$$A_{p_{11}} = A_{p_{22}} = \frac{E_p h_p}{(1-v_p^2)}, \qquad A_{p_{12}} = A_{p_{21}} = v_p A_{p_{11}}, \qquad A_{p_{33}} = \frac{1-v_p}{2} A_{p_{11}},$$

$$D_{p_{11}} = D_{p_{22}} = \frac{E_p h_p^3}{12(1-v_p^2)}, \qquad D_{p_{12}} = D_{p_{21}} = v_p D_{p_{11}}, \qquad D_{p_{33}} = \frac{1-v_p}{2} D_{p_{11}},$$

$$[\mathbf{C}_m] = \begin{bmatrix} \partial[\mathbf{H}_u(x,y)]/\partial x \\ \partial[\mathbf{H}_v(x,y)]/\partial y \\ \partial[\mathbf{H}_u(x,y)]/\partial y + \partial[\mathbf{H}_v(x,y)]/\partial x \end{bmatrix}, \qquad [\mathbf{C}_b]_k = \begin{bmatrix} -\partial^2[\mathbf{H}_w(x,y)]/\partial x^2 \\ -\partial^2[\mathbf{H}_w(x,y)]/\partial y^2 \\ -2\partial^2[\mathbf{H}_w(x,y)]/\partial x\,\partial y \end{bmatrix}.$$

E_p is the Young's Modulus of the plate, h_p is the thickness of the plate, v_p is the Poisson's ratio of the plate, $Area_p$ is the area of the plate element. The subscript p represents plate.

The mass matrix for the plate element can be derived in the same manner. Like the displacement, the acceleration at any point within the element can be related to the nodal accelerations by using the interpolation functions in equation (1). The mass matrix for the plate element can be formulated in the form

$$[\mathbf{m}_p] = \int\int_{Area_p} \begin{bmatrix} [\mathbf{F}_m][\mathbf{T}_m] & [\mathbf{0}] \\ [\mathbf{0}] & [\mathbf{F}_b][\mathbf{T}_b] \end{bmatrix}^{\mathrm{T}} \rho_p \begin{bmatrix} [\mathbf{F}_m][\mathbf{T}_m] & [\mathbf{0}] \\ [\mathbf{0}] & [\mathbf{F}_b][\mathbf{T}_b] \end{bmatrix} \mathrm{d}y\ \mathrm{d}x, \tag{4}$$

where

$$[\mathbf{F}_m]\begin{bmatrix} \mathbf{H}_u(x,y) \\ \mathbf{H}_v(x,y) \end{bmatrix}, \qquad [\mathbf{F}_b] = \begin{bmatrix} H_w(x,y) \\ \partial H_w(x,y)/\partial x \\ \partial H_w(x,y)/\partial y \end{bmatrix}.$$

ρ_p is the density of the plate.

3. STIFFENER ELEMENT FORMULATION

The stiffener element introduced in this section is based on the method described in Reference [1]. The stiffness and mass element matrices for a stiffener not aligned to the nodal lines are derived here (see Figure 2). The strain–displacement relation of the stiffener is given by

$$\begin{Bmatrix} \epsilon_t \\ \epsilon_n \\ \gamma_{tn} \end{Bmatrix} = \begin{Bmatrix} \partial u'/\partial t \\ \partial v'/\partial n \\ \partial u'/\partial n + \partial v'/\partial t \end{Bmatrix} + z \begin{Bmatrix} -\partial^2 w/\partial t^2 \\ -\partial^2 w/\partial n^2 \\ -2\partial^2 w/\partial t\,\partial n \end{Bmatrix}, \tag{5}$$

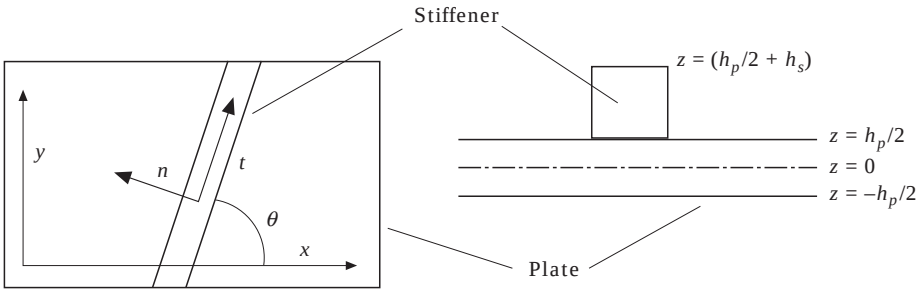

Figure 2. Description of arbitrarily oriented stiffener.

where u' is the axial extension along the stiffener, v' is the extension perpendicular to the stiffener, n is the direction perpendicular to the stiffener and t is the direction parallel to the stiffener. The inplane forces and bending moments in n, t co-ordinates are given by

$$\begin{Bmatrix} N_t \\ N_n \\ N_{tn} \\ M_t \\ M_n \\ M_{tn} \end{Bmatrix} = \begin{matrix} [\mathbf{A}_S] & [\mathbf{B}_S] \\ [\mathbf{B}_S] & [\mathbf{D}_S] \end{matrix} \begin{Bmatrix} \partial u'/\partial t \\ \partial v'/\partial n \\ \partial u'/\partial n + \partial v'/\partial t \\ -\partial^2 w/\partial t^2 \\ -\partial^2 w/\partial n^2 \\ -2\partial^2 w/\partial t\,\partial n \end{Bmatrix}, \tag{6}$$

where

$$A_{s_{11}} = A_{s_{22}} = E_s h_s/(1 - v_s^2), \qquad A_{s_{12}} = A_{s_{21}} = v_s A_{s_{11}}, \qquad A_{s_{33}} = (1 - v_s/2)A_{s_{11}},$$

$$B_{s_{11}} = B_{s_{22}} = E_s \left\{ \left(\frac{h_p}{2} + h_s \right)^2 - \left(\frac{h_p}{2} \right)^2 \right\} \Big/ 2(1 - v_s^2), \qquad B_{s_{12}} = B_{2_{21}} = vB_{s_{11}},$$

$$B_{s_{33}} = (1 - v_s)/2B_{s_{11}}, \qquad D_{s_{11}} = D_{s_{22}} = E_s \left\{ \left(\frac{h_p}{2} + h_s \right)^3 - \left(\frac{h_p}{2} \right)^3 \right\} \Big/ 3(1 - v_s^2),$$

$$D_{s_{12}} = D_{2_{21}} = v_s D_{s_{11}}, \qquad D_{s_{33}} = (1 - v_s)/2D_{s_{11}}.$$

E_s is the Young's modulus of the stiffener, h_s is the thickness of the stiffener. The subscript s represents stiffener.

Because the stiffener is considered as a beam, it can be assumed $N_n = N_{tn} = M_n = \partial v'/\partial n = \partial u'/\partial n + \partial v'/\partial t = 0$. Using this assumption, equation (6) can be reduced to

$$\begin{Bmatrix} N_t \\ M_t \\ M_{tn} \end{Bmatrix} = \begin{bmatrix} [\hat{\mathbf{A}}_s] & [\hat{\mathbf{B}}_s] \\ [\hat{\mathbf{B}}_s] & [\hat{\mathbf{D}}_s] \end{bmatrix} \begin{Bmatrix} \partial u'/\partial t \\ -\partial^2 w/\partial t^2 \\ -2\partial^2 w/\partial t\, \partial n \end{Bmatrix}, \tag{7}$$

where

$$\begin{bmatrix} [\hat{\mathbf{A}}_s] & [\hat{\mathbf{B}}_s] \\ [\hat{\mathbf{B}}_s] & [\hat{\mathbf{D}}_s] \end{bmatrix} = \begin{bmatrix} A_{s_{11}} - B_{s_{12}}(B_{s_{12}}/D_{s_{22}}) & B_{s_{11}} - B_{s_{12}}(D_{s_{21}}/D_{s_{22}}) & B_{s_{16}} - B_{s_{12}}D_{s_{26}}/D_{s_{22}} \\ B_{s_{11}} - D_{s_{12}}(B_{s_{12}}/D_{s_{22}}) & D_{s_{11}} - D_{s_{12}}(D_{s_{21}}/D_{s_{22}}) & D_{s_{16}} - D_{s_{12}}D_{s_{26}}/D_{s_{22}} \\ B_{s_{16}} - D_{s_{26}}(B_{s_{12}}/D_{s_{22}}) & D_{s_{16}} - D_{s_{26}}(D_{s_{21}}/D_{s_{22}}) & D_{s_{66}} - D_{s_{26}}D_{s_{26}}/D_{s_{22}} \end{bmatrix}.$$

The strains can be expressed in the x-y co-ordinates as

$$\partial u'/\partial t = (\partial u'/\partial x)\partial x/\partial t + (\partial u'/\partial y)\partial y/\partial t, \tag{8}$$

where

$$u' = u\cos\theta + v\sin\theta, \qquad \partial x/\partial t = \cos\theta, \qquad \partial y/\partial t = \sin\theta.$$

The displacement in equation (8) may be expresed in terms of the x and y co-ordinates as

$$\partial u'/\partial t = \partial u/\partial x\cos^2\theta + (\partial v/\partial y)\sin^2\theta + \tfrac{1}{2}(\partial u/\partial y + \partial v/\partial x)\sin 2\theta. \tag{9}$$

Similarly,

$$\partial^2 w/\partial t^2 = (\partial^2 w/\partial x^2)\cos^2\theta + (\partial^2 w/\partial y^2)\sin^2\theta + (\partial^2 w/\partial x\,\partial y)\sin 2\theta, \tag{10}$$

and

$$\partial^2 w/\partial t\,\partial n = \tfrac{1}{2}(-\partial^2 w/\partial x^2 + \partial^2 w/\partial y^2)\sin 2\theta + (\partial^2 w/\partial x\,\partial y)(-\sin^2\theta + \cos^2\theta). \tag{11}$$

Rearranging equations (9)–(11) gives

$$\begin{Bmatrix} \partial u'/\partial t \\ -\partial^2 w/\partial t^2 \\ -2\partial^2 w/\partial t\,\partial n \end{Bmatrix} = [\mathbf{C}\theta] \begin{Bmatrix} \dfrac{\partial u}{\partial x} \\ \dfrac{\partial v}{\partial y} \\ \dfrac{\partial u}{\partial y} + \dfrac{\partial v}{\partial x} \\ -\dfrac{\partial^2 w}{\partial x^2} \\ -\dfrac{\partial^2 w}{\partial y^2} \\ -2\dfrac{\partial^2 w}{\partial x\,\partial y} \end{Bmatrix} \tag{12}$$

where

$$[\mathbf{C}\theta] = \begin{bmatrix} \cos^2\theta & \sin^2\theta & 1/2\sin 2\theta & 0 & 0 & 0 \\ 0 & 0 & 0 & -\cos^2\theta & -\sin^2\theta & -(1/2)\sin 2\theta \\ 0 & 0 & 0 & \sin 2\theta & -\sin 2\theta & \sin^2\theta - \cos^2\theta \end{bmatrix}$$

The element stiffness matrix of the stiffener, like the element stiffness matrix of the plate, can be given by

$$[\mathbf{k}_s] = \int\int_{Area_s} \begin{bmatrix} [\mathbf{C}_m][\mathbf{T}_m] & [0] \\ [\mathbf{0}] & [C_b][T_b] \end{bmatrix}^{\mathrm{T}} [\mathbf{C}\theta]^{\mathrm{T}} \begin{bmatrix} [\hat{\mathbf{A}}_s] & [\hat{\mathbf{B}}_s] \\ [\hat{\mathbf{B}}_s] & [\hat{\mathbf{D}}_s] \end{bmatrix} [\mathbf{C}\theta] \begin{bmatrix} [\mathbf{C}_m][\mathbf{T}_m] & [\mathbf{0}] \\ [\mathbf{0}] & [\mathbf{C}_b][\mathbf{T}_b] \end{bmatrix} \mathrm{d}x\ \mathrm{d}y. \tag{13}$$

The displacement field at any point within the element in terms of nodal displacement is given by

$$\begin{Bmatrix} u \\ v \\ w \end{Bmatrix}_s = \begin{Bmatrix} u' - z\,\partial w'/\partial t \\ -z\,\partial w'/\partial n \\ w' \end{Bmatrix} = [\mathbf{G}] \begin{Bmatrix} u' \\ v' \\ w' \\ \partial w'/\partial t \\ \partial w'/\partial n \end{Bmatrix}, \tag{14}$$

where

$$[\mathbf{G}] = \begin{bmatrix} 1 & 0 & 0 & -z & 0 \\ 0 & 0 & 0 & 0 & -z \\ 0 & 0 & 1 & 0 & 0 \end{bmatrix}$$

and $Area_s$ = area of the stiffener element

As with equation (12), the displacement vector in equation (14) can be expressed in x-y co-ordinates as

$$\begin{Bmatrix} u \\ v \\ w \end{Bmatrix}_s = [\mathbf{G}]\,[\mathbf{F}\theta] \begin{Bmatrix} u \\ v \\ w \\ \partial w/\partial x \\ \partial w/\partial y \end{Bmatrix}$$

where

$$[\mathbf{F}\theta] = \begin{bmatrix} \cos\theta & \sin\theta & 0 & 0 & 0 \\ -\sin\theta & \cos\theta & 0 & 0 & 0 \\ 0 & 0 & 1 & 0 & 0 \\ 0 & 0 & 0 & \cos\theta & \sin\theta \\ 0 & 0 & 0 & -\sin\theta & \cos\theta \end{bmatrix}.$$

From the above equations the mass matrix can be written as

$$[\mathbf{m}_s] = \int_{Area_s}\int \begin{bmatrix} [\mathbf{C}_m][\mathbf{T}_m] & [\mathbf{0}] \\ [\mathbf{0}] & [\mathbf{C}_b][\mathbf{T}_b] \end{bmatrix}^{\mathrm{T}} [\mathbf{F}\theta]^{\mathrm{T}} \rho_s [\mathbf{G}]^{\mathrm{T}} [\mathbf{G}][\mathbf{F}\theta] \begin{bmatrix} [\mathbf{C}_m][\mathbf{T}_m] & [\mathbf{0}] \\ [\mathbf{0}] & [\mathbf{C}_b][\mathbf{T}_b] \end{bmatrix} \mathrm{d}x\ \mathrm{d}y, \tag{16}$$

where ρ_s is the density of the stiffener. By summing up the contributions from all of the plate and stiffener elements derived in equations (3), (4), (13) and (16), and taking account of the kinematic boundary conditions, the natural frequencies and mode shapes of the stiffened enclosure plate can be given by the following eigenvalue problem,

$$\omega_{PQ}^2 [\mathbf{M}]\{\mathbf{\Phi}^{PQ}\} = [\mathbf{K}]\{\mathbf{\Phi}^{PQ}\} \tag{17}$$

where $\{\mathbf{\Phi}^{PQ}\}$ is the (P, Q) mode shape vector of the enclosure plate (normalized with the maximum transverse displacement to unity), ω_{PQ} is the corresponding resonant frequency; [**M**] and [**K**] are the system mass and stiffness matrices of an enclosure plate with stiffeners.

4. ACOUSTIC VELOCITY POTENTIAL

An enclosure system similar to that of reference [14] is shown in Figure 1. The boundaries at $z = 0$, $z = c$ are flexible so that they can vibrate in typical mode shapes while the other walls are acoustically rigid. The acoustic velocity potential within the rectangular cavity is given by the following homogeneous wave equation [17],

$$\nabla^2\phi - (1/C_a^2)(\partial^2\phi/\partial t^2) = 0 \tag{18}$$

where ϕ is the velocity potential function and C_a is the speed of sound.

The vibration velocities in the x, y and z directions and pressures within the air cavity can be derived from the following equations,

$$\dot{X} = \partial\phi/\partial x, \qquad \dot{Y} = \partial\phi/\partial y, \qquad \dot{Z} = \partial\phi/\partial z, \qquad P = -\rho_a \partial\phi/\partial t. \tag{19}$$

where ρ_a is the density of air.

The boundary conditions of the rectangular cavity to be satisfied are (i) at $x = 0$ and $x = a$, $\dot{X} = \partial\phi/\partial x = 0$; (ii) at $y = 0$ and $y = b$, $\dot{Y} = \partial\phi/\partial y = 0$; (iii) at $z = 0$, $\dot{Z} = \partial\phi/\partial z = \dot{w}_{sou}(x, y, t)$; (iv) at $z = c$, $\dot{Z} = \partial\phi/\partial z = \dot{w}_{enc}(x, y, t)$.

Here $w_{sou}(x, y, t)$ and $w_{enc}(x, y, t)$ are the displacements of the source plate and the enclosure plate, so their velocities are marked with an overdot. The subscripts *enc* and *sou* represent the enclosure and source plates respectively.

By applying boundary conditions (i) and (ii), the solution of equation (17) is expressed [2, 3] as

$$\phi = \sum_{U=0}^{\bar{U}} \sum_{W=0}^{\bar{W}} \cos\left(\frac{U\pi x}{a}\right) \cos\left(\frac{W\pi y}{b}\right) \left[L^{UW} \cosh(\mu^{UW} z) + N^{UW} \sinh(\mu^{UW} z) \right] \mathrm{e}^{\mathrm{i}\omega t}, \tag{20}$$

where

$$\mu^{UW} = \sqrt{C_a^2((U\pi/a)^2 + (W\pi/b)^2) - \omega^2/C_a}.$$

a and b are the length and width of the enclosure plate, respectively; $\bar{U}$ and $\bar{W}$ are the numbers of the acoustic modes in the x and y directions; L^{UW} and N^{UW} are coefficients which depend on the boundary conditions at $z = 0$ and $z = c$.

5. ACOUSTIC–STRUCTURAL BOUNDARY CONDITIONS

In this section, the two variables, L^{UW} and N^{UW} in equation (19) are rewritten in terms of ω_{sou}^{ST} and ω_{enc}^{PQ}, the modal amplitudes of the source plate and the enclosure plate. Then, the velocity potential and the pressure within the air cavity can also be in terms of them. It is assumed that (P, Q) is the dominant mode shape of the enclosure plate and the source plate is forced to vibrate in the (S, T) mode shape with constant velocity. The profiles of the displacements of the source plate and the enclosure plate are given by

$$w_{sou}^{ST}(x, y, t) = \omega_{sou}^{ST}\psi^{ST}(x, y)\,\mathrm{e}^{\mathrm{i}\omega t}, \qquad w_{enc}^{PQ}(x, y, t) = \omega_{enc}^{PQ}\varphi^{PQ}(x, y)\,\mathrm{e}^{\mathrm{i}\omega t}, \tag{21, 22}$$

where $\psi^{ST}(x, y)$ and $\varphi^{PQ}(x, y)$ are the (S, T) mode shape of the source plate and (P, Q) mode shape of the enclosure plate respectively; ω_{sou}^{ST} and ω_{enc}^{PQ} are the modal amplitudes of the (S, T) mode of the source plate and (P, Q) mode of the enclosure plate, respectively.

The *in-vacuo* mode shapes of the source plate and the enclosure plate are found by using the finite element method introduced in the previous section. In other words, $\psi^{ST}(x, y)$ and $\varphi^{PQ}(x, y)$ are not analytical and derived from the interpolation of the transverse displacements in the (P, Q) mode shape vector $\{\mathbf{\Phi}^{PQ}\}$. By substituting equations (20, 22) into the boundary conditions (iii), (iv), the two variables, L_{UW} and N_{UW} can be rewritten in terms of $\mathscr{W}_{sou}^{ST}$ and $\mathscr{W}_{enc}^{PQ}$. The velocity potential in equation (20) within the rectangular air cavity can be expressed in terms of the modal displacement amplitudes of the source and enclosure plates. $\mathscr{W}_{sou}^{ST}$ and $\mathscr{W}_{enc}^{PQ}$.

$$\phi = \mathrm{i}\omega\,\mathrm{e}^{\mathrm{i}\omega t}\sum_{U=0}^{\bar{U}}\sum_{W=0}^{\bar{W}}\cos\left(\frac{U\pi x}{a}\right)\cos\left(\frac{W\pi y}{b}\right)$$

$$\times\left[\frac{(B^{PQ,UW}\mathscr{W}_{enc}^{PQ} - \alpha^{ST,UW}\mathscr{W}_{sou}^{ST}\cosh(\mu^{UW}c))}{\mu^{UW}\sinh(\mu^{UW}c)}\cosh(\mu^{UW}z)\right.$$

$$\left.+\frac{\alpha_{UW}^{ST}\mathscr{W}_{sou}^{ST}}{\mu^{UW}}\sinh(\mu^{UW}z)\right], \tag{23}$$

where

$$\alpha^{ST,UW} = \int_0^a\int_0^b \psi^{ST}(x, y)\cos\left(\frac{U\pi x}{a}\right)\cos\left(\frac{W\pi x}{b}\right)\mathrm{d}x\,\mathrm{d}y$$

$$\Big/ \int_0^a \int_0^b \cos\left(\frac{U\pi x}{a}\right)^2 \cos\left(\frac{W\pi x}{b}\right)^2 \mathrm{d}x\,\mathrm{d}y,$$

$$\beta^{PQ,UW} = \int_0^a \int_0^b \varphi^{PQ}(x, y) \cos\left(\frac{U\pi x}{a}\right) \cos\left(\frac{W\pi x}{b}\right) \mathrm{d}x\,\mathrm{d}y$$

$$\Big/ \int_0^a \int_0^b \cos\left(\frac{U\pi x}{a}\right)^2 \cos\left(\frac{W\pi x}{b}\right)^2 \mathrm{d}x\,\mathrm{d}y.$$

Using equations (19) and (23), the pressure at the $z = c$ is given by

$$P_c = \mathrm{e}^{\mathrm{i}\omega t} \sum_{U=0}^{\bar{U}} \sum_{W=0}^{\bar{W}} (\mathscr{W}_{enc}^{PQ} \Lambda_{enc}^{PQ,UW} - \mathscr{W}_{sou}^{PQ} \Lambda_{sou}^{ST,UW}) \cos\left(\frac{U\pi x}{a}\right) \cos\left(\frac{W\pi y}{b}\right), \quad (24)$$

where

$$\Lambda_{enc}^{PQ,UW} = \rho_a \omega^2 \beta^{PQ,UW} \cosh(\mu^{UW} c)/\mu^{UW} \sinh(\mu^{UW} c),$$
$$\Lambda_{sou}^{ST,UW} = \rho_a \omega^2 \alpha^{ST,UW}/\mu^{UW} \sinh(\mu^{UW} c).$$

6. RESPONSE OF STRUCTURAL VIBRATION

Consider the air pressure at the surface $z = c$, which is induced by the constant vibration motion of the source plate. The parameters of the enclosure plate, such as stiffness and mass etc., are used for evaluating the vibration displacement amplitudes of the source plate and the enclosure plate, $\mathscr{w}_{sou}^{ST}$ and $\mathscr{w}_{enc}^{PQ}$. Then, the modal equation of the forced motion of the enclosure plate due to the acoustical pressure at $z = c$ is

$$([\mathbf{K}] - \omega^2[\mathbf{M}])\{\mathbf{\Phi}^{PQ}\}\mathscr{W}_{enc}^{PQ} = \{\mathbf{F}\} = \begin{Bmatrix} \mathbf{F}_m = 0 \\ F_b \end{Bmatrix} \quad (25)$$

where $\{\mathbf{F}_m\}$ is the external membrane force vector and equal to zero because the only external force is the sound pressure at $z = c$ which is perpendicular to the enclosure plate; and $\{\mathbf{F}_b\}$ is the external bending force vector due to the sound pressure at $z = c$.

By using equations (1), (2) and (24), the bending force vector can be expressed in terms of $\mathscr{w}_{sou}^{ST}$ and $\mathscr{w}_{enc}^{PQ}$ as the following

$$\{\mathbf{F}_b\} = \sum^{NE} \int_{Area_i} [\mathbf{T}_b]^{\mathrm{T}} [\mathbf{H}_w(x, y)]^{\mathrm{T}} P_c \,\mathrm{d}A$$

$$-\mathrm{e}^{\mathrm{i}\omega t} \sum_{U=0}^{U=\bar{U}} \sum_{W=0}^{W=\bar{W}} (\mathscr{w}_{enc}^{PQ} \Lambda_{enc}^{PQ,UW} - \mathscr{w}_{sou}^{ST} \Lambda_{sou}^{ST,UW}) \{\mathbf{F}_{cos}^{UW}\}, \quad (26)$$

where

$$\{\mathbf{F}_{cos}^{UW}\} = \sum^{NE} \int_{Area_i} [\mathbf{T}_b]^{\mathrm{T}} [\mathbf{H}_w(x, y)]^{\mathrm{T}} \cos\left(\frac{U\pi x}{a}\right) \cos\left(\frac{W\pi y}{b}\right) \mathrm{d}A.$$

$Area_i$ is the area of the ith finite element on the enclosure plate; NE is the number of the finite elements of the mesh, and here the summation sign represents the assembly procedure to sum up the contributions from all element force vectors. The subscript cos represents pressure force of the double cosine distribution in equation (24).

The total force vector may also be expressed in terms of $\hat{w}_{sou}^{ST}$ and $\hat{w}_{enc}^{PQ}$ as the following

$$\{\mathbf{F}\} = \begin{Bmatrix} 0 \\ \mathbf{F}_b \end{Bmatrix} = -\mathrm{e}^{\mathrm{i}\omega t} \sum_{U=0}^{U=\bar{U}} \sum_{W=0}^{W=\bar{W}} (\hat{W}_{enc}^{PQ} \Lambda_{enc}^{PQ,UW} - \hat{W}_{enc}^{PQ} \Lambda_{sou}^{ST,UW}) \begin{Bmatrix} 0 \\ \mathbf{F}_{cos}^{UW} \end{Bmatrix}. \tag{27}$$

In the above formulation, $\hat{W}_{enc}^{PQ}$ can be seen as the modal co-ordinate. To perform modal reduction, the ratio of $\hat{W}_{enc}^{PQ}$ to $\hat{W}_{sou}^{ST}$ can be found by substituting equation (27) into equation (25) and multiplying $\lfloor \mathbf{\Phi}^{PQ} \rfloor$ on both sides and is given by

$$\frac{\hat{W}_{enc}^{PQ}}{\hat{W}_{sou}^{ST}} = \left(\sum_{U=0}^{\bar{U}} \sum_{W=0}^{\bar{W}} Z_{sou}^{ST,PQ,UW} \right) \Bigg/ \left(Z_{enc}^{PQ} + \sum_{U=0}^{\bar{U}} \sum_{W=0}^{\bar{W}} Z_{cav}^{PQ,UW} \right), \tag{28}$$

where

$$Z_{enc}^{PQ} = (\bar{K}^{PQ} - \omega^2 \bar{M}^{PQ}) + \mathrm{i}\bar{C}^{PQ}, \qquad Z_{cav}^{PQ,UW} = \Lambda_{enc}^{PQ,UW} \lfloor \mathbf{\Phi}^{PQ} \rfloor \begin{Bmatrix} 0 \\ \mathbf{F}_{cos}^{UW} \end{Bmatrix},$$

$$Z_{sou}^{ST,PQ,UW} = \Lambda_{sou}^{ST,UW} \lfloor \mathbf{\Phi}^{PQ} \rfloor \begin{Bmatrix} 0 \\ \mathbf{F}_{cos}^{UW} \end{Bmatrix}, \qquad (\bar{K}^{PQ}, \bar{M}^{PQ}) = \lfloor \mathbf{\Phi}^{PQ} \rfloor ([\mathbf{K}] \quad [\mathbf{M}]) \{\mathbf{\Phi}^{PQ}\}.$$

$\bar{C}^{PQ}$ is the modal damping which has been added into equation (28) and equal to $2\sqrt{\bar{K}^{PQ}\bar{M}^{PQ}}\xi^{PQ}$, ξ^{PQ} is the modal damping ratio of the (P, Q) mode of the enclosure plate; the subscript cav represents the enclosure cavity.

Using the relation between acoustic and vibration by the well-known Rayleigh's formula [18], one knows that

$$\text{S.E.} = \sigma \times \text{V.E.} \tag{29}$$

where S.E. is measured. The far field sound energy, V.E. is vibration energy, and σ is the radiation efficiency of the vibration source.

Using equations (28) and (29), the sound insertion loss is defined by

$$\text{IL} = -10 \log (\text{S.E.}_{enc}/\text{S.E.}_{sou}) = -10 \log (|\hat{W}_{enc}^{PQ}/\hat{W}_{sou}^{ST}|^2 \sigma^{PQ}/\sigma^{ST})$$

$$-10 \log \left(\left| \left(\sum_{U=0}^{\bar{U}} \sum_{W=0}^{\bar{W}} Z_{sou}^{ST,PQ,UW} \right) \Bigg/ \left(Z_{enc}^{PQ} + \sum_{U=0}^{\bar{U}} \sum_{W=0}^{\bar{W}} Z_{cav}^{PQ,UW} \right) \right|^2 \frac{\sigma^{PQ}}{\sigma^{ST}} \right), \tag{30}$$

where S.E.$_{sou}$ and S.E.$_{enc}$ are the sound energies radiated by the enclosed source and enclosure plates, respectively; and σ^{PQ} is the radiation efficiency of the (P, Q) mode and is given in reference [18].

Neglecting the cross-coupling effects between the structural modes of the enclosure plate, equation (30) can be rewritten into a more general form as reference [8]

$$\mathrm{IL} = -10 \log \left\{ \sum_{P=1}^{\bar{P}} \sum_{Q=1}^{\bar{Q}} \left(\left| \frac{\mathscr{W}_{enc}^{PQ}}{\mathscr{W}_{sou}^{ST}} \right|^2 \frac{\sigma^{PQ}}{\sigma^{ST}} \right) \right\}, \tag{31}$$

where $\bar{P}$ and $\bar{Q}$ are the structural mode numbers of the enclosure plate.

7. THEORETICAL RESULTS

Mukherjee [1] investigated the free vibration of stiffened plates. They considered a square plate with a central stiffener (see Figure 3) and solved for natural frequencies using an eight-node isoparametric quadratic plate element with 40 degrees of freedom. In Table 1, the natural frequencies obtained by the four-node C^1 conforming rectangular plate element are presented and compared with those results from Mukherjee [1]. The analysis is performed employing symmetry and antisymmetry conditions along the centerlines. A quarter of the plate is modelled using a 5×5 mesh. It can be seen that good correlation exists among the results. In Table 2, the symmetric mode natural frequencies are plotted against different mesh sizes. It can be seen that the 8×8 mesh natural frequencies have a maximum difference of 2% when compared with the 10×10 mesh result. In the following cases, the mesh size of 8×8 for a quarter of the plate is chosen.

The insertion losses of an aluminium enclosure plate with different cavity depths are shown in Figure 4. The material properties of the aluminium plate are as follows: Young's modulus $= 7{\cdot}1 \times 10^{10}$ Pa, density $= 2700$ kg/m^3, Poisson's ratio $= 0{\cdot}3$, modal damping ratio $= 0{\cdot}02$. The predictions are based on the source plate vibrating in the (1, 1) mode and the enclosure plate vibrating in symmetric

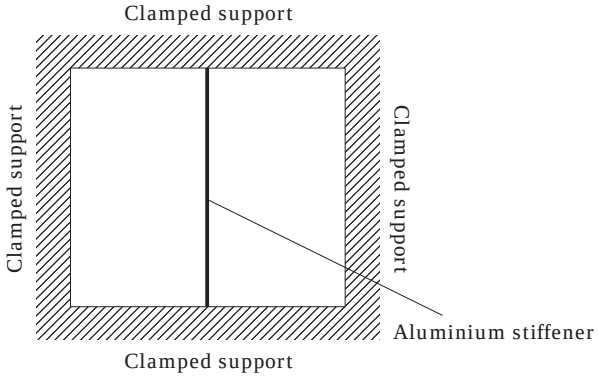

Figure 3. Clamped support aluminium plate with a stiffener: plate dimensions $0{\cdot}203$ m $\times$ $0{\cdot}203$ m $\times$ $0{\cdot}00137$ m; aluminium stiffener $0{\cdot}00635$ m $\times$ $0{\cdot}01133$ m $\times$ $0{\cdot}203$ m.

TABLE 1

Frequencies (Hz) for the centrally stiffened clamped plate

Mode	Mukherjee [1]	Present	Difference (%)
1	711·8	727·2	2·12
2	768·2	768·2	0·03
3	1016·5	1014·4	0·21
4	1031·9	1029·9	0·19
5	1465·2	1448·4	1·16
6	1476·5	1454·7	1·50
7	1743·8	1664·9	4·74
8	1866·3	1878·8	0·67
9	2109·1	2059·8	2·39
10	2117·2	2063·4	2·60
11	2264·1	2250·5	0·60
12	2296·3	2277·8	0·81
13	2505·8	2462·1	1·77
14	2779·9	2685·5	3·53
15	2820·9	2708·6	4·15
16	2933·3	2848·7	2·97

mode shapes. Smaller cavity depth can also make the structural resonance frequency higher. On the other hand, cavity depth is an important factor which can largely affect insertion loss at low frequencies. It can be seen that at the

TABLE 2

Mesh convergence study of symmetric mode resonant frequencies (Hz) for the centrally stiffened clamped plate

Symmetric Mode	Mesh size							
	3 × 3	4 × 4	5 × 5	6 × 6	7 × 7	8 × 8	9 × 9	10 × 10
1	772·7	769·4	768·2	767·6	767·3	767·1	766·9	766·9
2	1464·8	1457·0	1454·7	1453·7	1453·3	1453·1	1452·9	1452·9
3	1712·5	1678·6	1664·9	1658·0	1654·0	1651·4	1649·7	1648·5
4	2508·0	2479·9	2462·1	2454·1	2450·0	2447·6	2446·1	2445·0
5	2763·2	2722·5	2708·6	2703·1	2700·6	2699·2	2698·4	2697·9
6	2903·2	2870·0	2851·1	2843·7	2840·4	2838·8	2837·8	2837·3
7	4150·8	4069·4	4039·5	4028·1	4023·0	4020·4	4018·9	4018·0
8	5034·3	4308·0	4289·6	4262·3	4249·0	4242·1	4238·4	4236·2
9	5369·1	4691·5	4640·7	4611·2	4597·1	4589·9	4585·7	4583·2
10	5711·2	5000·5	4973·0	4934·4	4915·9	4906·6	4901·5	4898·5
11	6681·5	6039·2	5964·3	5929·6	5913·9	5906·0	5901·6	5899·0
12	6825·9	6161·9	6016·8	6064·9	6045·3	6035·3	6029·8	6026·6
13	9128·1	7839·4	6900·7	6887·2	6840·1	6813·3	6798·1	6789·2
14	9609·7	8033·8	7200·0	7134·3	7081·3	7051·7	7034·5	7023·8
15	9733·0	8107·4	7762·2	7752·8	7689·5	7654·3	7634·5	7622·9
16	10423·2	8645·6	7987·7	7924·0	7894·9	7880·3	7872·2	7867·5

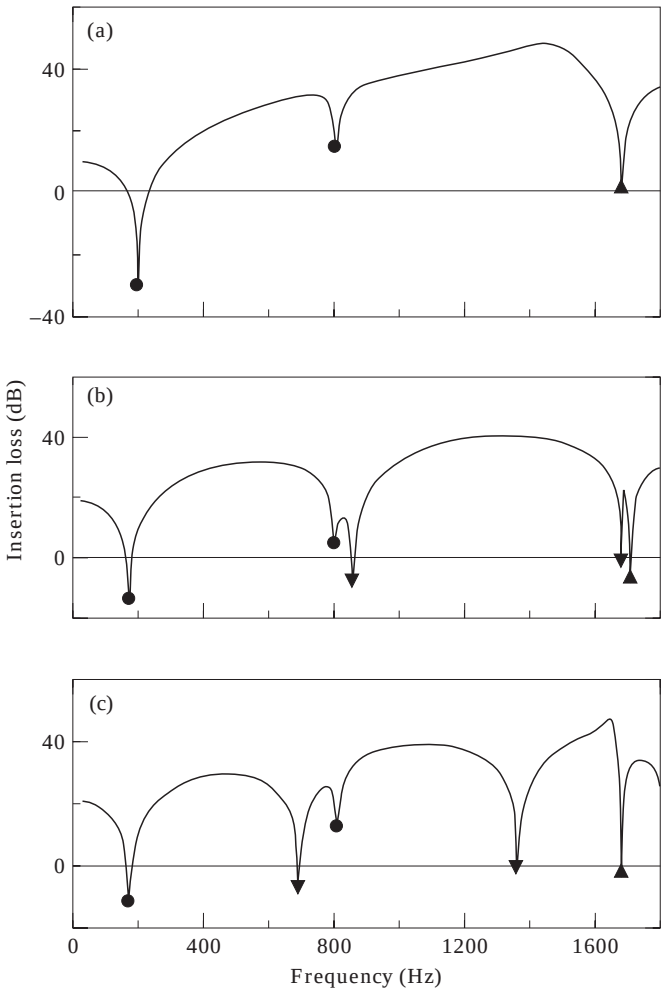

Figure 4. Simply supported aluminium plate (0·203 m × 0·203 m × 0·00137 m): source plate mode shape, (1, 1) mode. Cavity depths: (a) 0·05 m; (b) 0·2 m and (c) 0·25 m. Key: ●, (1, 1) or (3, 1) structural mode resonance; ▼, acoustic resonance in the z direction; (2, 0) or (0, 2) acoustic resonance in the x-y plane.

frequencies below the structural resonance, it is noted that greater cavity depth results in higher insertion loss. In the frequencies ranging from 800–900 Hz, the structural resonance of the (1, 3) mode of the enclosure plate in the second figure in Figure 4 is close to the acoustical resonance. This makes the two resonances form a ''wider and deeper'' dip. In each case, the acoustic resonance parallel to the source plate is unchanged being independent of the cavity depth and the stiffness of the enclosure plate. Among the three cases, the case with shorter depth has higher frequency resonance in the z direction.

In Figure 5, the predictions are based on the source plate vibrating in the (2, 1) mode and the enclosure plate vibrating in anti-symmetrical modes. Unlike the acoustic (2, 0) mode in Figure 4, the (0, 1) acoustic mode in Figure 5 imposes greater effect on insertion loss than the structural mode.

In Figure 6, the effect of the boundary conditions of the enclosure plate on the insertion loss is presented. The insertion loss above the fundamental resonant frequency of the clamped case is slightly lower than that of the simply supported case. Below this frequency, boundary conditions appear to have a considerable effect on the insertion loss in that the insertion loss of the clamped plate is higher than that of the simply supported plate. The enclosure plate with a stiffener has a higher fundamental resonant frequency, when compared with the plates without any stiffener (the location and dimensions of the stiffener is the same as that of the one shown in Figure 3). At the frequencies below the fundamental resonance, the stiffener of the enclosure plate makes the insertion loss much higher than those of the other two enclosure plates. Above this frequency however, the coupling effect between the structural and acoustic modes has a significant effect, resulting in a lower insertion loss.

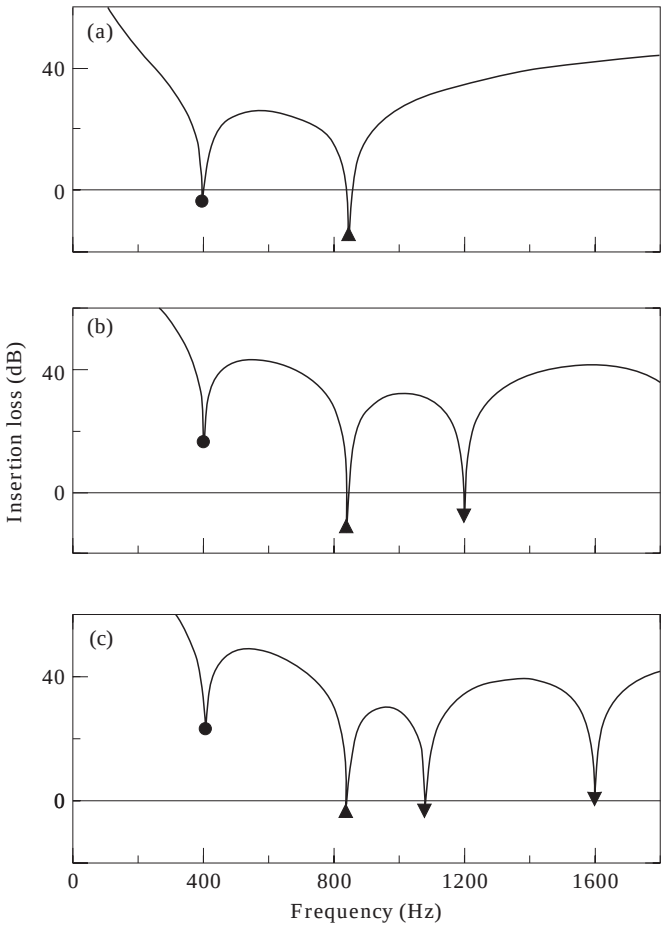

Figure 5. Simply supported aluminium plate (0·203 m × 0·203 m × 0·00137 m): source plate mode shape, (2, 1) mode. Cavity depths: (a) 0·05 m; (b) 0·2 m and (c) 0·25 m. Key: ●, (2, 1) structural mode resonance; ▼, acoustic resonance in the z direction; ▲, (1, 0) or (0, 1) acoustic resonance in the x-y plane.

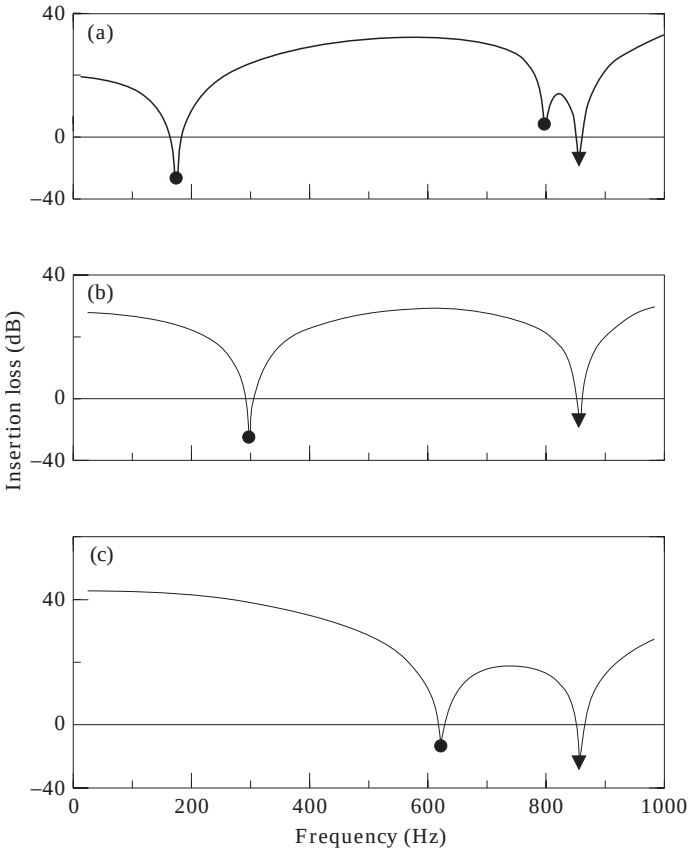

Figure 6. Aluminium plate (0·203 m × 0·203 m × 0·00137 m): source plate mode shape (1, 1) mode, cavity depth 0·2 m. (a) Simply supported without stiffener; (b) clamped without stiffener and (c) clamped with stiffener. Key: ●, (1, 1) structural mode resonance; ▼, acoustic resonance in the z direction.

8. EXPERIMENTAL RESULTS

In Figures 7a and 7b, the theoretical insertion loss predictions of the 1 mm steel panel, and the 3 mm aluminium plate with a stiffener which measures 2 cm × 3 cm × 70 cm, are confirmed experimentally over the frequency range. The location of the stiffener is bonded along the center line of the 3 mm aluminium plate. The material properties of the aluminium plate are as follows: Young's modulus = $7{\cdot}1 \times 10^{10}$ Pa, density = 2700 kg/m^3, Poisson's ratio = 0·3, modal damping ratio = 0·02. The material properties of the steel plate are as follows: Young's modulus = 20×10^{10} Pa, density = 7800 kg/m^3, Poisson's ratio = 0·3, modal damping ratio = 0·02. The boundary conditions are assumed to be simply supported in the theoretical prediction. The resonance frequencies of the two enclosure panels are somewhat different from the predicted values because of the uncertainties in the boundary conditions and the bonding between the stiffener and aluminium plate. This would not make a large difference between the prediction

and measurement because the experimental data were measured with one-third octave filtered white noise (i.e., the average insertion loss over each frequency band is given). Since the main uncertainty remains in the damping ratio of the model, poor insertion loss predictions occur at the resonant frequencies. Overall, the trends of the theoretical predictions in the two cases agree reasonably well with the experimental results. It can be seen in both cases that the coupling effect between the (1, 0) acoustical mode and the (2, 1) structural mode is an important factor which can cause deterioration of the insertion loss performance of an enclosure plate (see the dip in Figure 7a around 500 Hz and the other dip in Figure 7b around 250 Hz).

In Figure 8, the effect of the stiffener on the insertion loss performance of the 3 mm aluminium plate is shown and compared with mass law. It is not surprising according to the numerical results on Figure 6a that a higher insertion loss results from the application of the stiffener. In other frequencies, the stiffener cannot act as an efficient method of enhancing the insertion loss ability of the aluminium enclosure plate and the insertion loss can be less than predicted by mass law.

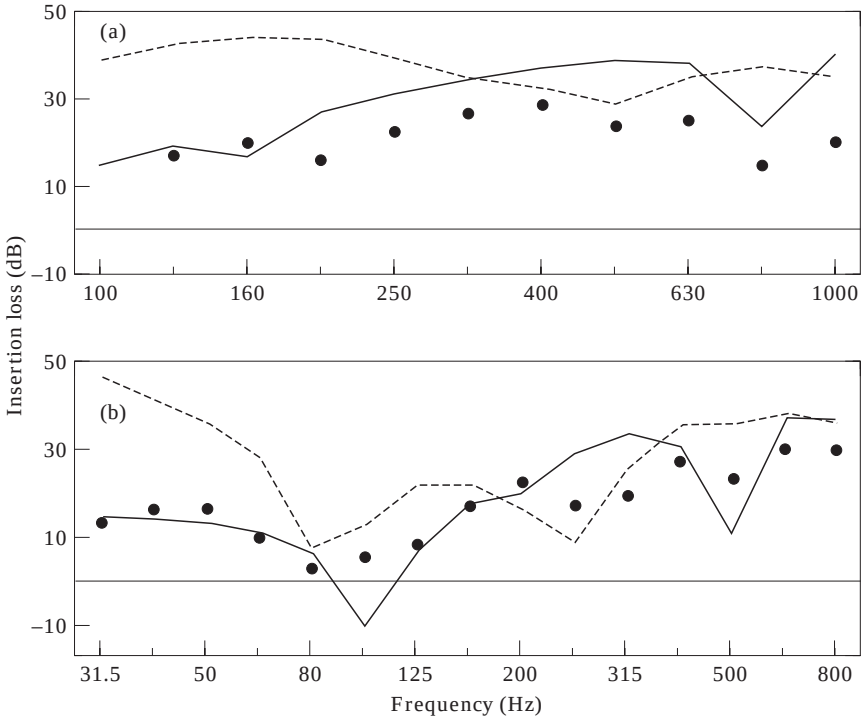

Figure 7. Comparison of measured and predicted of insertion loss of (a) the 1 mm steel plate; dimensions of the enclosure plate 0·37 m × 0·37 m; cavity depth 0·21 m, (b) the 3 mm aluminium plate with a stiffener; dimensions of the enclosure plate 0·72 m × 0·72 m; cavity depth 0·16 m. Key: ●, measured data; —, numerical data using symmetrical structural modes; - - - - -, numerical prediction using antisymmetrical structural modes.

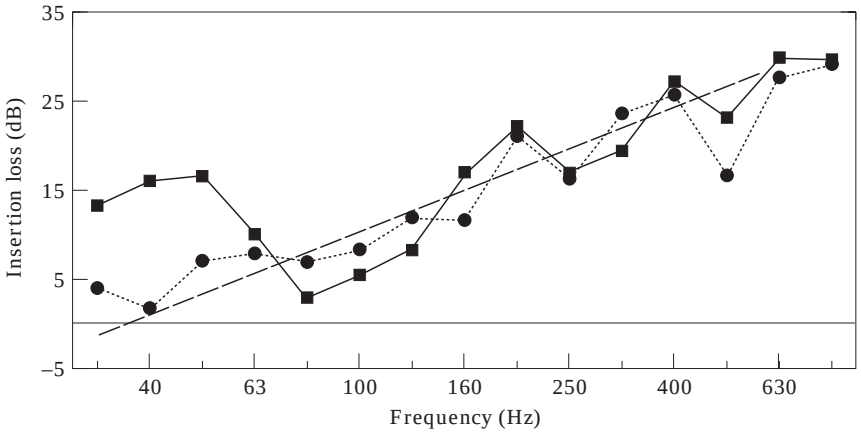

Figure 8. Comparison of measured insertion loss of the two enclosure plates with dimensions 0·72 m × 0·72 m; cavity depth 0·16 m. Key: –■–, 3 mm aluminium plate with stiffener; · · · · ● · · · ·, 3 mm aluminium plate without stiffener; – – –, mass law.

9. CONCLUSION

A model for predicting the insertion loss of a stiffened enclosure panel has been presented. The results of the measurements made to test the validity of the model suggest it can give a reasonable prediction. From both the theoretical and experimental data, it can be concluded that; 1) the couping effect between the (1, 0) acoustical mode and the (2, 1) structural mode is an important factor which can cause deterioration of the insertion loss of an enclosure plate; 2) stiffeners can be used to enhance the insertion loss ability of an enclosure plate at the frequencies below the fundamental resonance. However, at other frequencies, the enclosure plate could give worse insertion loss performance.

ACKNOWLEDGMENT

The research was sponsored by PolyV Grant No. 351/233.

REFERENCES

1. A. Mukherjee and M. Mukhopadhyay 1988 *Computers and Structures* **30**, 1303–1317. Finite element free vibration of eccentrically stiffened plates.
2. Y. Y. Lee and C. F. Ng 1994 *The Fifth International Conference on Recent Advances in Structural Dynamics*, *ISVR*, *UK*, *July*, 1023–1032. The prediction of the effects of stiffness and damping on noise reduction of small enclosures.
3. Y. Y. Lee 1995 *M.Phil. Thesis*, *Department of Civil and Structural Engineering*, *The Hong Kong Polytechnic University*. Structural–acoustic analysis of close-fitting enclosures.
4. Y. Y. Lee and C. F. Ng 1995 *Proceeding of The International Conference on Structural Dynamics*, *Vibration*, *Noise and Control*, *Hong Kong*, *Dec*. 1201–1206. The noise and vibration reduction of close fitting curved enclosure panels.
5. Y. Y. Lee and C. F. Ng 1997 *Journal of Building Acoustics* **2**, 549–567. The effects of coupled source/cavity modes on the acoustic insertion loss of close-fitting enclosures.

6. Y. Y. Lee and C. F. Ng 1997 *The Sixth International Conference on Recent Advances in Structural Dynamics*, *ISVR*, *UK*, *July*, 553–562. Insertion loss of stiffened enclosures.
7. R. H. Lyon 1963 *Journal of the Acoustical Society of America* **35**, 1791–1797. Noise reduction of rectangular enclosures with one flexible wall.
8. A. J. Pretlove 1965 *Journal of Sound and Vibration* **2**, 197–209. Free vibrations of a rectangular plate backed by a closed rectangular cavity.
9. R. S. Jackson 1966 *Journal of Sound and Vibration* **3**, 82–94. Some aspects of the performance of acoustic hoods.
10. R. W. Guy 1973 *Journal of Sound Vibration* **27**, 207–223. The transmission of sound through a cavity-backed finite plate.
11. E. H. Dowell, G. F. Gorman and D. A. Smith 1977 *Journal of sound and Vibration* **52**, 519–242. Acoustoelasticity: general theory, acoustical natural modes and forced response to sinusoidal excitation, including comparisons with experiment.
12. S. Narayanan and R. L. Shanbhag 1988 *Journal of Sound and Vibration* **150**, 251–270. Sound transmission through elastically supported sandwich panels into a rectangular enclosure.
13. D. J. Oldham and S. N. Hillarby 1991 *Journal of Sound and Vibration* **150**, 261–281. The acoustical performance of small close fitting enclosures, part 1: theoretical models.
14. D. J. Oldham and S. N. Hillarby 1991 *Journal of Sound and Vibration* **150**, 283–300. The acoustical performance of small close fitting enclosures, part 2: experimental investigation.
15. J. N. Reddy 1985 *Shock and Vibration Digest* **17**, 3–8. A review of the literature on finite element modeling of laminated composite plates.
16. K. C. Rockey, H. R. Evans, D. W. Griffiths, D. A. Nethercot 1983 *The Finite element Method*. Granada Publishing.
17. G. F. Carrier 1988 *Partial Differential Equations*, *Theory and Technique*, New York: Academic Press; second edition.
18. C. E. Wallace 1972 *Journal of the Acoustical Society of America* **51**, 946–952. Radiation Resistance of a Rectangular Panel.

APPENDIX

The element used in the finite element model is a rectangular element consisting of twenty-four structural degrees of freedom, accounting for bending and membrane displacements. The rectangular element consists of four corner nodes with displacements w, u, v and their derivatives $w_{,x}$, $w_{,y}$, $w_{,xy}$. Co-ordinate transformations are required to relate the local element co-ordinates to the global structural co-ordinates. The membrane nodal displacements are given by

$$\{\mathbf{w}_m\} = \lfloor u_1 \quad u_2 \quad u_3 \quad u_4 \quad v_1 \quad v_2 \quad v_3 \quad v_4 \rfloor^{\mathrm{T}} \tag{A1}$$

The nodal membrane displacements can be obtained by substituting the element nodal co-ordinates into appropriate approximation functions. Thus the membrane nodal displacements become

$$u(0, 0, t) = u_1 = b_1, \qquad u(a_e, 0, t) = u_2 = b_1 + b_2 a_e, \tag{A2, A3}$$

$$u(a_e, b_e, t) = u_3 = b_1 + b_2 a_e + b_3 b_e + b_4 a_e b_e, \tag{A4}$$

$$u(0, b_e, t) = u_4 = b_1 + b_3 b_e, \qquad v(0, 0, t) = v_1 = b_5, \qquad v(a_e, 0, t) = v_2 = b_5 + b_6 a_e,$$

$$v(a_e, b_e, t) = v_3 = b_5 + b_6 a_e + b_7 b_e + b_8 a_e b_e, \tag{A5–A7}$$

$$v(0, b_e, t) = v_4 = b_5 + b_7 b_e, \tag{A8, A9}$$

where the element length and width are a_e and b_e, respectively, and the generalized co-ordinates are represented by the b coefficients. The membrane displacements equations (A2)–(A9) may be written in matrix notation as $\{\mathbf{w}_m\} = [\mathbf{T}_m]^{-1}\{\mathbf{b}\}$ which is expressed as follows

$$\begin{Bmatrix} u_1 \\ u_2 \\ u_3 \\ u_4 \\ v_1 \\ v_2 \\ v_3 \\ v_4 \end{Bmatrix} = \begin{bmatrix} 1 & 0 & 0 & 0 & 0 & 0 & 0 & 0 \\ 1 & a_e & 0 & 0 & 0 & 0 & 0 & 0 \\ 1 & a_e & b_e & a_e b_e & 0 & 0 & 0 & 0 \\ 0 & 0 & b_e & 0 & 0 & 0 & 0 & 0 \\ 0 & 0 & 0 & 0 & 1 & 0 & 0 & 0 \\ 0 & 0 & 0 & 0 & 1 & a_e & 0 & 0 \\ 0 & 0 & 0 & 0 & 1 & a_e & a_e b_e & b_e \\ 0 & 0 & 0 & 0 & 1 & 0 & b_e & 0 \end{bmatrix} \begin{Bmatrix} b_1 \\ b_2 \\ b_3 \\ b_4 \\ b_5 \\ b_6 \\ b_7 \\ b_8 \end{Bmatrix}. \tag{A10}$$

Similarly the bending transformation is determined using the sixteen degrees of freedom. Thus the sixteen bending nodal displacements are

$$\{\mathbf{w}_b\} = \lfloor w_1 \quad w_2 \quad w_3 \quad w_4 \quad w_{1,x} \quad w_{2,x} \quad w_{3,x} \quad w_{4,x} \quad w_{1,y} \quad w_{2,y} \quad w_{3,y} \quad w_{4,y} \quad w_{1,xy} \quad w_{2,xy} \quad w_{3,xy} \quad w_{4,xy} \rfloor^{\mathrm{T}}. \tag{A11}$$

The displacements are approximated using the cubic polynomial. The derivative expressions are given by

$$w_{,x} = a_2 + 2a_4 + a_5 y + 3a_7 x^2 + 2a_8 xy + a_9 y^2 + 3a_{11} x^2 y + 2a_{12} xy^2 + a_{13} y^3 + 3a_{14} x^2 y^2 + 2a_{15} xy^3 + 3a_{16} x^2 y^3, \tag{A12}$$

$$w_{,y} = a_3 + a_5 x + 2a_6 y + a_8 x^2 + 2a_9 xy + 3a_{10} y^2 + a_{11} x^3 + 2a_{12} x^2 y + 3a_{13} xy^2 + 2a_{14} x^3 y + 3a_{15} x^2 y^2 + 3a_{16} x^3 y^2, \tag{A13}$$

$$w_{,xy} = a_5 + 2a_8 x + 2a_9 y + 3a_{11} x^2 + 4a_{12} xy + 3a_{13} y^2 + 6a_{14} x^2 y + 6a_{15} xy^2 + 9a_{16} x^2 y^2. \tag{A14}$$

The nodal bending displacements are obtained by substituting the nodal co-ordinates into equation (3.4) and equations (A12)–(A14). Thus the transverse displacements are given as

$$w(0, 0, t) = w_1 = a_1, \qquad w(a_e, 0, t) = w_2 = a_1 + a_2 a_e + a_4 a_e^2 + a_7 a_e^3, \quad \text{(A15, A16)}$$

$$\begin{aligned} w(a_e, b_e, t) = w_3 = {} & a_1 + a_2 a_e + a_3 b_e + a_4 a_e^2 + a_5 a_e b_e + a_6 b_e^2 \\ & + a_7 a_e^3 + a_8 a_e^2 b_e + a_9 a_e b_e^2 + a_{10} b_e^3 + a_{11} a_e^3 b_e \\ & + a_{12} a_e^2 b_e^2 + a_{13} a_e b_e^3 + a_{14} a_e^3 b_e^2 + a_{15} a_e^2 b_e^3 + a_{16} a_e^3 b_e^3, \end{aligned} \quad \text{(A17)}$$

$$w(0, b_e, t) = w_4 = a_1 + a_3 b_e + a_6 b_e^2 + a_{10} b_e^3. \quad \text{(A18)}$$

Likewise, the slopes with respect to the x-axis are

$$w_{,x}(0, 0, t) = w_{,x1} = a_2, \qquad w_{,x}(a_e, 0, t) = w_{,x2} = a_2 + 2a_4 a_e + 3a_7 a_e^2, \quad \text{(A19, A20)}$$

$$\begin{aligned} w_{,x}(a_e, b_e, t) = w_{,x3} = {} & a_2 + 2a_4 a_e + a_5 b_e + 3a_7 a_e^2 + 2a_8 a_e b_e + a_9 b_e^2 \\ & + 3a_{11} a_e^2 b_e + 2a_{12} a_e b_e^2 + a_{13} b_e^3 + 3a_{14} a_e^2 b_e^2 + 2a_{15} a_e b_e^3 + a_{16} a_e^2 b_e^3, \end{aligned} \quad \text{(A21)}$$

$$w_{,x}(0, b_e, t) = w_{,x4} = a_2 + a_5 b_e + a_9 b_e^2 + a_{13} b_e^3. \quad \text{(A22)}$$

The slopes with respect to the y-axis are

$$w_{,y}(0, 0, t) = w_{,y1} = a_3, \qquad w_{,y}(a_e, 0, t) = w_{,y2} = a_3 + a_5 a_e + a_8 a_e^2 + a_{11} a_e^3, \quad \text{(A23, A24)}$$

$$\begin{aligned} w_{,y}(a_e, b_e, t) = w_{,y3} = {} & a_3 + a_5 a_e + 2a_6 b_e + a_8 a_e^2 + 2a_9 a_e b_e + 3a_{10} b_e^2 \\ & + a_{11} a_e^3 + 2a_{12} a_e^2 b_e + 3a_{13} a_e b_e^2 + 2a_{14} a_e^3 b_e + 3a_{15} a_e^2 b_e^2 + 3a_{16} a_e^3 b_e^2, \end{aligned} \quad \text{(A25)}$$

$$w_{,y}(0, b_e, t) = w_{,y4} = a_3 + 2a_6 b_e + 3a_{10} b_e^2. \quad \text{(A26)}$$

The cross derivatives about the z-axis are

$$w_{,xy}(0, 0, t) = w_{,xy1} = a_5, \qquad w_{,xy}(a_e, 0, t) = w_{,xy2} = a_5 + 2a_8 a_e + 3a_{11} a_e^2, \quad \text{(A27, A28)}$$

$$\begin{aligned} w_{,y}(a_e, b_e, t) = w_{,y3} = {} & a_5 + 2a_8 a_e + 2a_9 b_e + 3a_{11} a_e^2 + 4a_{12} a_e b_e \\ & + 3a_{13} b_e^2 + 6a_{14} a_e^2 b_e + 6a_{15} a_e b_e^2 + 9a_{16} a_e^2 b_e^2, \end{aligned} \quad \text{(A29)}$$

$$w_{,y}(0, b_e, t) = w_{,y4} = a_5 + 2a_9 b_e + 3a_{13} b_e^2. \quad \text{(A30)}$$

Equations (A15)–(A30) may be expressed in matrix notation as $\{\mathbf{w}_b\} = [\mathbf{T}_b]^{-1}\{\mathbf{a}\}$ where $[\mathbf{T}_b]^{-1}$ is defined as

$$[\mathbf{T}_b]^{-1} = \begin{bmatrix}
1 & 0 & 0 & 0 & 0 & 0 & 0 & 0 & 0 & 0 & 0 & 0 & 0 & 0 & 0 & 0 \\
1 & a_e & 0 & a_e^2 & 0 & 0 & a_e^3 & 0 & 0 & 0 & 0 & 0 & 0 & 0 & 0 & 0 \\
1 & a_e & b_e & a_e^2 & a_e b_e & b_e^2 & a_e^3 & a_e^2 b_e & a_e b_e^2 & b_e^3 & a_e^3 b_e & a_e^2 b_e^2 & a_e b_e^3 & a_e^3 b_e^2 & a_e^2 b_e^3 & a_e^3 b_e^3 \\
1 & 0 & b_e & 0 & 0 & b_e^2 & 0 & 0 & 0 & b_e^3 & 0 & 0 & 0 & 0 & 0 & 0 \\
0 & 1 & 0 & 0 & 0 & 0 & 0 & 0 & 0 & 0 & 0 & 0 & 0 & 0 & 0 & 0 \\
0 & 1 & 0 & 2a_e & 0 & 0 & 3a_e^3 & 0 & 0 & 0 & 0 & 0 & 0 & 0 & 0 & 0 \\
0 & 1 & 0 & 2a_e & b_e & 0 & 3a_e^3 & 2a_e b & b_e^2 & 0 & 3a_e^2 b_e & 2a_e b_e^2 & b_e^3 & 3a_e^2 b_e^2 & 2a_e b_e^3 & 3a_e^2 b_e^3 \\
0 & 1 & 0 & 0 & b_e & 0 & 0 & 0 & b_e^2 & 0 & 0 & 0 & b_e^3 & 0 & 0 & 0 \\
0 & 0 & 1 & 0 & 0 & 0 & 0 & 0 & 0 & 0 & 0 & 0 & 0 & 0 & 0 & 0 \\
0 & 0 & 1 & 0 & a_e & 0 & 0 & a_e^2 & 0 & 0 & a_e^2 & 0 & 0 & 0 & 0 & 0 \\
0 & 0 & 1 & 0 & a_e & 2b_e & 0 & a_e^2 & 2a_e b_e & 3b_e^2 & a_e^3 & 2a_e^2 b_e & 3a_e b_e^2 & 2a_e^3 b_e & 3a_e^2 b_e^2 & 3a_e^3 b_e^2 \\
0 & 0 & 1 & 0 & 0 & 2b_e & 0 & 0 & 0 & 3b_e^2 & 0 & 0 & 0 & 0 & 0 & 0 \\
0 & 0 & 0 & 0 & 1 & 0 & 0 & 0 & 0 & 0 & 0 & 0 & 0 & 0 & 0 & 0 \\
0 & 0 & 0 & 0 & 1 & 0 & 0 & 2a_e & 0 & 0 & 3a_e^2 & 0 & 0 & 0 & 0 & 0 \\
0 & 0 & 0 & 0 & 1 & 0 & 0 & 2a_e & 2b_e & 0 & 3a_e^2 & 4a_e b_e & 3b_e^2 & 6a_e^2 b_e & 6a_e b_e^2 & 9a_e^2 b_e^2 \\
0 & 0 & 0 & 0 & 1 & 0 & 0 & 0 & 2b_e & 0 & 0 & 0 & 3b_e^2 & 0 & 0 & 0
\end{bmatrix}. \quad \text{(A31)}$$

The bending transformation matrix $[\mathbf{T}_b]$ therefore is obtained by inverting the matrix equation (A31).